

Implications for Galaxy Evolution from the Cosmic Evolution of Supernova Rate Density

Takeshi ODA¹, Tomonori TOTANI¹, Naoki YASUDA², Takahiro SUMI³,
Tomoki MOROKUMA⁵, Mamoru DOI⁴, George KOSUGI⁵

¹*Department of Astronomy, School of Science, Kyoto University, Sakyo-ku, Kyoto 606-8502, Japan*
takeshi@kusaastro.kyoto-u.ac.jp

²*Institute for Cosmic Ray Research, University of Tokyo, Kashiwa, Chiba, 227-8582, Japan*

³*Solar-Terrestrial Environment Laboratory, Nagoya University, Furo-cho, Chikusa-ku, Nagoya, 464-8601, Japan*

⁴*Institute of Astronomy, School of Science, University of Tokyo, 2-21-1 Osawa, Mitaka, Tokyo, 181-0015, Japan*

⁵*National Astronomical Observatory of Japan, 2-21-1 Osawa, Mitaka, Tokyo, 181-8588, Japan*

(Received ; accepted)

Abstract

We report a comprehensive statistical analysis of the observational data of the cosmic evolution of supernova (SN) rate density, to derive constraints on cosmic star formation history and the nature of type Ia supernova (SN Ia) progenitor. We use all available information of magnitude, SN type, and redshift information of both type Ia and core-collapse (CC) SNe in GOODS and SDF, as well as SN Ia rate densities reported in the literature. Furthermore, we also add 157 SN candidates in the past Subaru/Suprime-Cam data that are newly reported here, to increase the statistics. We find that the current data set of SN rate density evolution already gives a meaningful constraint on the evolution of the cosmic star formation rate (SFR) at $z \lesssim 1$, though strong constraints cannot be derived for the delay time distribution (DTD) of SNe Ia. We derive a constraint of $\alpha \sim 3-4$ [the evolutionary index of SFR density $\propto (1+z)^\alpha$ at $z \lesssim 1$] with an evidence for a significant evolution of mean extinction of CC SNe [$E(B-V) \sim 0.5$ at $z \sim 0.5$ compared with ~ 0.2 at $z = 0$], which does not change significantly within a reasonable range of various DTD models. This result is nicely consistent with the systematic trend of α estimates based on galactic SFR indicators in different wavelengths (ultraviolet, $H\alpha$, and infrared), indicating that there is a strong evolution in mean extinction of star forming regions in galaxies at relatively low redshift range of $z \lesssim 0.5$. These results are obtained by a method that is completely independent of galaxy surveys, and especially, there is no detection limit about the host galaxy luminosity in our analysis, giving a strong constraint on the star formation activity in high- z dwarf galaxies or intergalactic space.

Key words: supernovae:general — galaxies:evolution — cosmology:observations

1. INTRODUCTION

In recent years a number of searches for high redshift supernovae (SNe) have been conducted. Although the primary purpose of most of these surveys is measurement of the cosmic expansion, these surveys also allowed measurements of the cosmic supernova rate density and its evolution (Pain et al. 2002; Tonry et al. 2003; Madgwick et al. 2003; Gal-Yam & Maoz 2004; Blanc et al. 2004; Maoz & Gal-Yam 2004; Dahlen et al. 2004; Cappellaro et al. 2005; Barris and Tonry 2006; Neill et al. 2006; Poznanski et al. 2007; Sharon et al. 2007; Mannucci et al. 2007; Kuznetsova et al. 2007). Studying these data should provide us with important information not only for the cosmic star formation history (CSFH) but also the still unknown progenitor of type Ia supernovae (SNe Ia). The progenitor of SNe Ia is believed to be a binary system including a white dwarf, and the SN Ia rate density evolution is a convolution of the cosmic star formation history and the delay time distribution (DTD) from star formation to SN Ia events. DTD depends on the progenitor models, and hence to constrain DTD observationally is a useful approach to reveal the

SN Ia progenitor (Madau et al. 1998; Yungelson & Livio 1998, 2000; Dahlen & Fransson 1999; Gilliland et al. 1999; Gal-Yam & Maoz 2004; Strolger et al. 2004, 2005; Barris et al. 2004; Oda & Totani 2005, hereafter OT05; Strigari et al. 2005).

However, it is not an easy task to actually extract useful constraints from the SN rate density evolution data. Previous studies (Maoz & Gal-Yam 2004; Strolger et al. 2004; Förster et al. 2006) mainly concentrated on the determination of DTD, using the rate density evolution of SNe Ia. In such an analysis, sometimes CSFH models are assumed based on the observational estimates from high- z galaxy surveys. However, as argued by Förster et al. (2006), the constraint on DTD models sensitively depends on the assumed CSFH, and hence it is difficult to derive a robust constraint on DTD.

The primary purpose of this paper is to perform a comprehensive likelihood analysis using all available SN rate density evolution data in the literature, to derive constraints on DTD and/or CSFH. After the GOODS high- z supernova survey (Dahlen et al. 2004; Strolger et al. 2004), whose data was used in Strolger et al. (2004) and Förster

et al. (2006), a number of observational estimates of SN rate density evolution have been published (mostly for SNe Ia, but some data also for CC SNe). Our approach is to derive constraints only by using SN rate data, without using information of CSFH from galaxy surveys. We will perform a simultaneous fit to both the SN Ia and CC SN rate density evolution data, surveying parameters of the CSFH model with a variety of DTD models. We will find that, though a strong constraint on DTD models cannot be derived even from all the available data so far, we can set interesting constraints on CSFH and evolution of mean dust extinction of CC SNe, which can be compared with those inferred from galaxy surveys.

Although there are a number of observational estimates on CSFH at a variety of redshifts from galaxy surveys, there is still a large uncertainty in the star formation rate (SFR) density estimated from galaxy observations, because of extinction, initial mass function, or extrapolation of luminosity functions to fainter magnitudes below the detection limits (see Hopkins 2004 and Hopkins & Beacom 2006, and reference therein). Therefore it is useful and important to derive constraints on CSFH from SNe independently of galaxy surveys. In contrast to SFR density estimates by galaxies, detectability of SNe does not depend on the host galaxy brightness, and even intergalactic star formation activity can be probed by hostless SNe. Searches for $z \sim 1$ SNe are typically performed at wavelength around the i' and z' band roughly corresponding to the rest-frame visual bands, and hence the effect of extinction by dust is expected to be smaller than the CSFH estimates based on the rest-frame UV emission of galaxies. It is not trivial that a unit mass of star formation always produces the same number of SNe, but it could evolve with redshift or physical properties of galaxies. If a significant difference between CSFH inferred from galaxy surveys and that from SN surveys is found, it might indicate that the relation between star formation and supernova production is not as simple as normally assumed.

In addition to the available SN rate density data in the literature, we also utilize the photometric sample of SN candidates found in the past observations using Subaru/Suprime-Cam. This Subaru Supernova Survey (SSS) sample includes 157 supernova candidates, 61 out of which have clear offsets from the centers of host galaxies and hence they are most likely SNe. This data set is complementary to GOODS, SNLS and the IfA deep survey (Strolger et al. 2004; Neill et al. 2006; Barris and Tonry 2006) in terms of the combination of the survey area and depth; the covered area of SSS, 1.4 deg^2 , is wider than the GOODS, and the SSS depth, $i' \sim 26.0$, is deeper than the SNLS and the IfA deep survey. Though no SN type or redshift information is available for the SSS sample, we add this data set to our likelihood analysis to increase the statistics especially for CC SNe. Compared with SNe Ia, there are not many data of the rate density for CC SNe. Combined analysis of the SSS counts including all SNe and other data for SN Ia rate density evolution should give some constraints on the CC SN rate density evolution and hence CSFH.

The following are the plan of this paper. In §2 and §3 we describe the SSS data set and analysis procedure of selecting SN candidates. Formulations of the comparison of the theoretical model and the observational data are given in §4. Constraints on the CSFH from our comprehensive parameter survey are derived in §5. Conclusions are given in §6. Throughout this paper, the standard Λ CDM universe is assumed with the following values of the cosmological parameters: $\Omega_M = 0.3$, $\Omega_\Lambda = 0.7$, $h_{70} \equiv H_0 / (70 \text{ km s}^{-1} \text{ Mpc}^{-1}) = 1$. All magnitudes are given in the AB magnitude system.

2. The SSS Data

The SSS data set consists of the following three fields, named A2152, MS1520.1, and the spring field (SF), whose positions on the sky are given in Table 1. All images are taken with the Subaru/Suprime-Cam (Miyazaki et al. 2002) having an effective field-of-view (FOV) of $30' \times 24'$, with a time interval of about one month that is suitable for a high- z supernova search. We describe details of the observations at each field below.

A2152 field – A single FOV of the Suprime-Cam centered on the galaxy cluster Abell 2152 was observed, where two galaxy clusters (A2152 at $z = 0.04$ and A2152-B at $z = 0.13$) closely overlap on the line of sight (Blakeslee et al. 2001). About one month after the first imaging of this field (2003 May 5), the field was imaged again during four consecutive nights (June 1–4). Images were taken with V_c and I_c band filters and typical exposure time is a few hours for each filter per day, but we use only the I_c band images for our supernova search. About 40 % of supernova candidates found in I_c band data of this field were not detected on V_c band images, while there is no SN candidate that was detected only in V_c band.

MS1520.1 field – A single FOV of the Suprime-Cam was observed around the galaxy cluster MS1520.1+3002 at $z = 0.117$ (Stocke et al. 1991). Observations were performed on April 25 and May 20 in 2001 with the i' band filter. The exposure time is about one hour.

It should be noted that the expected number of supernovae in the galaxy clusters in the MS 1520.1 and A2152 fields is too small to affect the conclusions of this paper (Gal-Yam et al. 2002; Sharon et al. 2007), and hence the existence of these clusters is not taken into account in our theoretical modeling.

The spring field – There are four adjacent Suprime-Cam images of this field in i' band, which we call SF 1–4. The first images were taken on March 19, and the second and third ones were on April 9 and 11, in 2002. Typical exposure time of each field is about one hour, but the observational conditions of SF2 and SF3 are better than those of SF1 and SF4. This field and the MS1520.1 field were observed as a part of the Supernova Cosmology Project. Thus, the observation was designed to find high redshift SNe Ia for the cosmological purpose, and follow-up spectroscopic observations of some supernova candidates were performed. As a result, three SNe (2002fc, 2002fd and 2002fe) are clearly identified to be SNe Ia, and another

SN (2002ff) is a possible candidate of SN Ia. Their redshifts are 0.88, 0.278, 1.086, and 1.1, respectively. (See IAU circ. 7971 for more details.) All of these are included in our SN candidates, but the information obtained with spectroscopic follow-up is not used, because the majority of the SNe in the SSS sample do not have spectroscopic information, and adding these spectroscopic information hardly affects the conclusions of this paper.

3. Selection of the SSS Supernova Candidates

Here we describe how we selected supernova candidates from the SSS data in detail, and a schematic flow-chart of these processes is presented in Fig. 1.

3.1. Variable Object Detection, Detection Efficiency and Position Accuracy

First, we made differential images from image pairs separated by about one month, using the image subtraction method ISIS (Alard & Lupton 1998; Alard 2000). Source detection was carried out using the SExtractor software (Bertin & Arnouts 1996). We detected candidate variable objects requiring that they have five or more connected pixels whose counts are more than 1σ level of the surface brightness fluctuation, after $0''.7$ FWHM Gaussian smoothing on the subtracted images. The variability magnitude (m_{var}) corresponding to the flux on the subtracted image was measured by the SExtractor’s automatic aperture magnitude. From these candidates, objects having high signal-to-noise (S/N) were selected. The criteria are $S/N = 7 - 10$, which depend on observational conditions of the fields. Finally we checked the images of these objects on the subtracted and original frames by eye in order to eliminate spurious objects.

The detection efficiency $\varepsilon(m_{\text{var}})$ and the position accuracy of variable objects on the subtracted images are estimated by simulations using artificial point sources placed randomly on one of the pre-subtraction images, under the exactly same object selection criteria as described above. Ideally, this test should be performed on various background conditions (e.g., in the blank field or on a host galaxy), since the detection efficiency could be changed by the location of variable sources. However, we ignore this effect in this paper, because the typical surface brightness of supernova host galaxies at $z \gtrsim 0.5$ is fainter than the sky level, and hence the noise of image is dominated by the sky background. In fact, we confirmed that there is no marked difference in the fluctuation of photon counts of the subtracted image between the blank field and locations of galaxies having typical magnitudes of supernova hosts. This result is in agreement with previous studies (e.g., Strolger et al. 2004; Poznanski et al. 2007). Following Strolger et al. (2004), detection efficiency estimated for various magnitudes of flux variability is fitted by the following function:

$$\varepsilon(m_{\text{var}}) = \frac{1}{1 + \exp[(m_{\text{var}} - m_0)/S_{\text{fit}}]}. \quad (1)$$

We use a single value of $S_{\text{fit}} = 0.43$ for all fields, but differ-

ent values of m_0 are fitted to the simulations in different fields. The fitting results of m_0 are given in Table 2.

We estimate the accuracy of position recovery by measuring the positional offsets of detected objects from the original positions. As shown in Fig. 2, the offsets well obeys the two-dimensional Gaussian distribution. Their standard deviations in one dimension derived by least square fits are $\sigma = 0.34$ and 0.51 pixel for $m_{\text{var}} = 25.0$ and 25.8 , respectively, in the A2152 field ($1 \text{ pixel} = 0''.2$).

3.2. Host Galaxies

Many extragalactic variable objects should be associated with host galaxies, and their nature and positional relation to variable objects are important information to select supernovae. First we simply define a tentative host galaxy as the object in the reference image whose surface brightness peak is the closest to a detected variable object. Sometimes the host galaxies are classified as point sources (the SExtractor stellarity parameter greater than 0.8), and their positions are the same as those of variable point sources. In such cases they could be simply the variable sources such as QSOs or variable stars. Furthermore, we cannot exclude a possible contribution from unresolved host galaxies. In these cases, we assign the next closest object in the reference frame as the tentative host galaxies. Therefore, positions of the variable objects are always different from the centers of their tentative host galaxies by definition.

Based on the estimates of the position accuracy for variable objects, we call an object “on-center” when $d_p < 1.5$, where d_p is the distance from the center of host galaxies to variable objects measured in units of pixel. The center of host galaxies is simply defined by the surface brightness peak. About 97 % and 85 % of the bright ($m_{\text{var}} = 25.0$) and faint ($m_{\text{var}} = 25.8$) point sources are found within 1.5 pixels ($= 0''.3$) from the original position, respectively, according to the simulation using artificial sources in the A2152 field.

We define the distance between a variable object and its host galaxy center that is normalized by the size of the host galaxy, as $d_n \equiv d_p/r_{p,\text{gal}}$, where $r_{p,\text{gal}}$ is the effective size of the host galaxy, defined as the radius of the ellipse from the host center to the direction of the variable object. The ellipse is obtained by the fitting to the host galaxy, as calculated in the SExtractor, and its size is determined so that the squares of the major and minor axes are the same as the second order moments along the axes, i.e.,

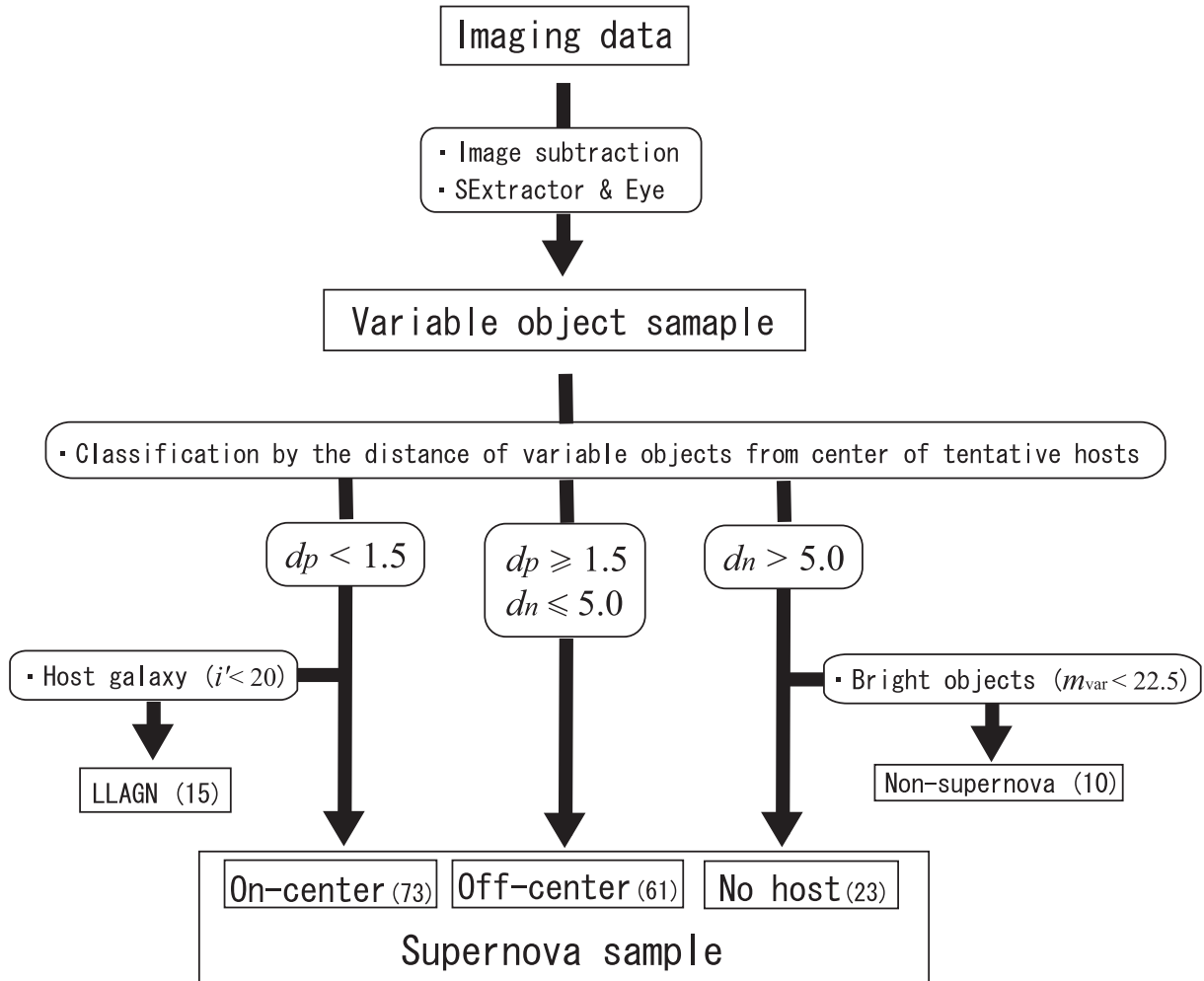
$$a_j^2 \equiv \frac{\sum_{i \in S} F_i x_{i,j}^2}{\sum_{i \in S} F_i}, \quad (2)$$

where the subscript i denotes for each pixel, F_i the flux counts in a pixel in I_c - (A2152 field) or i' -band (other fields), $x_{i,j}$ is the distance from the host center to the i -th pixel projected onto the major or minor axis (denoted by the subscript j), and the summation is over the whole region of the host galaxy.

Now we examine the d_n distribution of the tentative host galaxies, which is shown in Fig. 3. The distribution clearly shows a stronger correlation between variable

Table 1. Basic Information of the SSS Observations

Field name	R.A.	Decl.	Area [deg ²]	Observing dates	Typical exposure time (hour)	Band filter
A2152	16 ^h 05 ^m 22 ^s	+16°26'55"	0.21	2003 May 5, June 1-4	3	I_C, V_C
MS1520.1	15 ^h 22 ^m 13 ^s	+29°51'59"	0.23	2001 April 25, May 20	1	i'
SF 1	14 ^h 00 ^m 56 ^s	+05°40'48"	0.24	2002 March 19, April 9, 11	1	i'
SF 2	13 ^h 58 ^m 36 ^s	+05°22'30"	0.23	2002 March 19, April 9, 11	1	i'
SF 3	14 ^h 03 ^m 46 ^s	+05°11'04"	0.23	2002 March 19, April 9, 11	1	i'
SF 4	14 ^h 13 ^m 18 ^s	+05°40'43"	0.24	2002 March 19, April 9, 11	1	i'

**Fig. 1.** A flow-chart showing the detection and selection procedures of the supernova candidates in SSS.

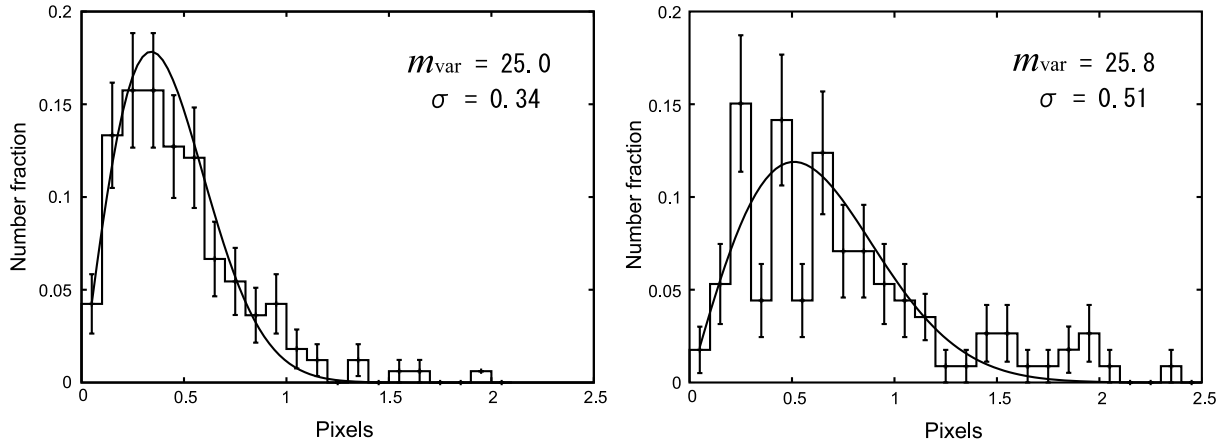


Fig. 2. Histograms of the distance between original and recovered positions of artificial point sources in the A2152 field. Left and right panels show the cases of two different magnitudes of the artificial sources ($m_{\text{var}} = 25.0$ and 25.8), respectively. Error bars show a 1σ statistical error. Solid lines are fits by two-dimensional Gaussian distribution [$\propto r \exp(-r^2/2\sigma^2)$] with $\sigma = 0.34$ and 0.51 pixel, respectively.

objects and host galaxies than that expected for objects that are randomly distributed on the sky, indicating that the majority of variable objects are physically associated with galaxies. The radial distribution of supernovae in their host galaxies is still uncertain (e.g., Bartunov et al. 1992; Howell et al. 2000), and here we test the galaxy surface brightness profiles often used in the literature, i.e., the exponential and the de Vaucouleurs profile. Here, we have taken into account the effect of seeing for the surface brightness profile, by relating the effective radius of the original profiles to the seeing-convolved second order moments. It should be noted that the simple exponential or de Vaucouleurs law may not be sufficient to describe all galaxies; there may be contribution from irregular galaxies, and cosmological surface brightness dimming effect may alter significantly the apparent profile (e.g., Totani & Yoshii 2000). However these effects are difficult to model quantitatively, and they are ignored here for the simplicity.

We find that the observed distribution is different from what expected when all variable objects obey the exponential or the de Vaucouleurs profile. However, the distribution is well described by the combination of the two components: a galaxy profile (exponential or de Vaucouleurs) and a random distribution. We find the best-fit relative proportion by the Kolmogorov-Smirnov test as 94 (88)% for the exponential (de Vaucouleurs) profile and the rest for a random distribution. The de Vaucouleurs profile gives an especially good fit to the observed distribution. However, it does not necessarily mean that the de Vaucouleurs profile is better than the exponential for SN distribution, since there may be a significant contribution from AGNs. From this figure, we find that almost all objects with $d_n > 5$ are likely to be unrelated to the tentatively assigned host objects, and hence we define objects with $d_n > 5$ as those without detectable host galaxies.

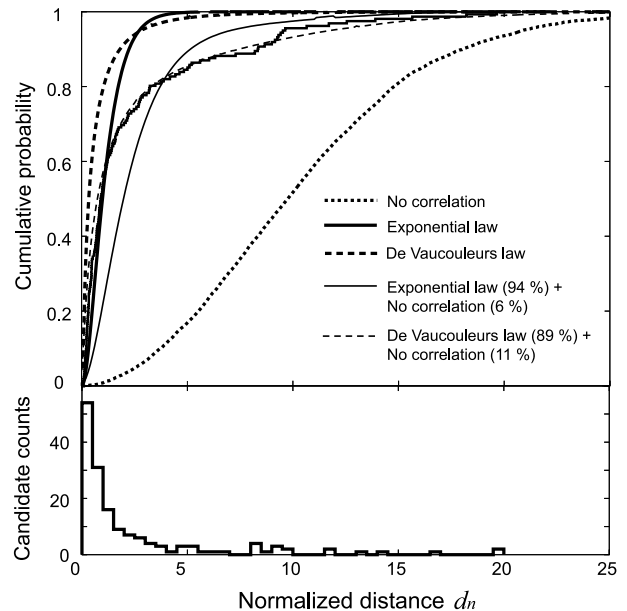


Fig. 3. Cumulative (top) and differential (bottom) distributions of the normalized distance d_n between the positions of variable objects and the centers of host galaxies. Model distributions derived from the exponential and de Vaucouleurs laws are shown with thick solid and dashed lines, respectively. The distribution expected for objects located randomly on the reference images is shown with the dotted line. The thin solid/dashed lines are the combined distribution of the exponential/de Vaucouleurs law and the random distribution. The relative proportions between the different components are indicated in the figure.

Table 2. Depth of surveys and number of detected SN candidates.

Field	m_0 [mag]	Number of SN candidates			
		All	On-center	Off-center	No host
A2152	25.8	33	12	17	4
MS1520.1	26.1	13	5	7	1
SF 1	25.3	20	11	5	4
SF 2	26.0	30	15	12	3
SF 3	26.0	41	20	15	6
SF 4	25.6	20	10	5	5
Total		157	73	61	23

3.3. The Supernova Candidates

3.3.1. Off-center Supernova Candidates

Now we have a robust sample of supernovae, i.e., the 61 variable objects associated with host galaxies and their locations are off-center on the host galaxies ($d_p > 1.5$ pix and $d_n \leq 5$). Because of these properties, the majority of them should be supernovae rather than AGNs. A possible contamination is chance superpositions of background AGNs in front of unrelated foreground galaxies (Gal-Yam et al. 2007). We can make a rough estimate of such events as follows. From the statistics of a similar variable object search by Morokuma et al. (2007) using the Subaru XMM-Newton Deep Survey (SXDS) data set, about 40 AGNs are expected in the SSS data. The surface area covered by galaxies with a similar magnitude to that of host galaxies in the SSS is about 5% of the total survey area, and hence we expect a few random superpositions. This number is much smaller than the off-center supernova candidates, and hence this effect can be neglected.

3.3.2. On-center Supernova Candidates

When variable objects are on the center of their host galaxies, we cannot discriminate between the two possibilities of supernovae or AGNs. However, some of these objects show very faint variability flux compared with the total magnitude of the host galaxies, and these objects are most likely to be low-luminosity AGNs (LLAGNs) with very low accretion rate as reported in Totani et al. (2005), because supernovae are generally as bright as the brightest class of galaxies. In fact, we found no off-center SN candidates associated with galaxies brighter than $i' = 20$. Therefore we removed 15 variable objects that are located at the center of very bright galaxies ($i' < 20$).

The remaining 73 on-center variable objects are then called as “on-center supernova candidates”, though we cannot exclude a contamination of AGNs in this sample. However, if we assume that supernovae trace the light of the host galaxies, we can estimate the expected number of on-center supernovae from the number of off-center supernovae, by extrapolation of a surface brightness profile. We find that 32 and 129 on-center supernovae are expected for the exponential and de Vaucouleurs profiles, respectively. The reality is likely between the two, and if we assume the Sérsic profile, we find that the expected number becomes the same as the observed number with the Sérsic’s index of $n_{\text{ser}} \sim 3$. These results indicate that at least about half of the on-center objects are supernovae (correspond-

ing to the exponential profile). In fact, as mentioned in the previous subsection, we expect about 40 AGNs in the SSS from the statistics of the SXDS variable object search (Morokuma et al. 2007), i.e., about a half of the on-center candidates.

The effect of AGN contamination in the on-center sample will be examined when we will compare the theoretical model of supernova rate evolution to the observed data.

3.3.3. No-host Supernova Candidates

The variable objects without host galaxies should also be examined since supernovae may be included in them. First we notice that there are objects that are clearly much brighter than expected for supernovae. In the off-center supernova sample, there is no object brighter than $m_{\text{var}} = 22.5$ in the variability magnitude. However, 10 objects in the no-host sample are brighter than this magnitude in spite of the no-detection of a host. These objects are most likely variable quasars or variable stars in our Galaxy, and hence they are rejected from the supernova candidates.

Then, the remaining 23 objects are defined as the no-host supernova candidates without detectable host galaxies, and there is no marked difference between the variability magnitude distributions of this sample and the off-center supernovae. Thus, although we cannot exclude significant contamination from quasars and Galactic variable stars, most of these are possibly supernovae with host galaxies that are fainter than the detection threshold ($i' = 25.0$) or truly intergalactic supernovae. To examine the former possibility, we estimate $\eta(z)$, which is the fraction of supernovae in host galaxies that are detectable by SSS. We assume that the supernova rate in a galaxy is proportional to the rest-frame V -band luminosity of a host galaxy. This is an assumption that should not be accurately correct; CC SNe are expected to trace galactic light in shorter wavelength such as rest-frame UV, and SNe Ia with a long delay time would trace longer wavelength light that is related to the stellar mass. However, our data set is limited about available band filters, and we make this assumption for the present data set.

Then we can estimate $\eta(z)$ by the V -band luminosity function of galaxies at a given z and the SSS detection limit for galaxies. We assume the following values and redshift evolution of the Schechter parameters of the luminosity function: $\alpha = -1.15 - \log(1 + z)$ and $M_* = -20.5 - 5.0 \log(1 + z)$, from the observations by Ilbert et al. (2005). The K-correction between the ob-

served band (i' or I) and the rest-frame V are calculated assuming the Sbc galaxy template. The calculated correction factors in this way is $\eta = 0.90, 0.79$ and 0.72 for $z = 0.5, 0.8,$ and $1.0,$ respectively. The typical redshifts of SNe that should be detectable in SSS is ~ 0.5 and 1.0 for CC SNe and SNe Ia, respectively, and we detected 134 supernova candidates with detectable host galaxies. Therefore, most or perhaps all of the 23 no-host candidates can be explained by those associated with galaxies under the detection limit. In other words, there is no evidence for a significant population of intergalactic supernova population.

3.4. Summary of SN Candidate Selections

As a result of the above selection procedures, we find 157 supernova candidates in total, including 73 on-center, 61 off-center, and 23 no-host candidates. Images of representative objects of these classification are given in Fig. 4, as well as the images of those classified as non-SNe objects. A summary of the results for each field is presented in Table 2. The distribution of the variability magnitude of these supernova candidates is shown in Fig. 5, as well as the estimated detection efficiency. The behavior of the faint end of the distribution is in reasonable agreement with the detection efficiency estimate. No considerable field-to-field variation is found.

3.5. The Sample Used for the Statistical Analysis

In the following likelihood analysis including the SSS data, we will present two cases of (i) using all of the on- and off-center SSS samples and (ii) using only the off-center SSS sample. In the former case, all on-center and off-center SN candidates are assumed to be the real supernovae. In the latter case, the effect of the removal of central regions of host galaxies is corrected assuming that the supernova distribution obeys the exponential profile as calculated in §3.3.2. For this correction we simply multiplied a factor of 0.65 to the theoretical prediction of the cosmic SN rate density, since the mean fraction of light in central regions of all host galaxies in the SSS is 0.35. As described in §3.3.2, the exponential profile corresponds to assuming that about half of on-center candidates are the real supernovae. Since the exponential profile is the least concentrated one among the various profiles assumed in the literature, the reality should be between the above two cases and hence we can check the systematic uncertainty about the AGN contamination by this treatment.

We do not include the no-host supernova candidates in the following analysis, since we cannot exclude the contamination by variable quasars or Galactic variable stars in this sample. We have already shown in §3.3.3 that the number of no-host candidates is similar to that expected by SNe with host galaxies under the detection limit, and hence there is no evidence for a significant population of truly intergalactic supernovae. Therefore, we only make a correction for SNe that are classified as no-host because their host galaxies are fainter than the detection limit, by using the quantity $\eta(z)$ calculated in §3.3.3. This correction factor is not far from unity, and it does not signifi-

cantly affect our conclusions even if this effect is completely ignored.

4. Theoretical Model of SN Rate Evolution

4.1. Cosmic Star Formation History

For the parametrization of CSFH, we use the following functional form (Gal-Yam & Maoz 2004):

$$\Phi(z) \propto \left[\left(\frac{1+z_{\text{break}}}{1+z} \right)^{5\alpha} + \left(\frac{1+z_{\text{break}}}{1+z} \right)^{5\beta} \right]^{-0.2}. \quad (3)$$

Here, α and β are indices of the CSFH at low and high redshift, respectively. The CC SN rate evolution is simply assumed to be proportional to the CSFH, because of their short life. The SN Ia rate density $r_{\text{Ia}}(z)$ is calculated from the CSFH convolved with the DTD, $f_D(t_{\text{Ia}})$, where the delay time t_{Ia} is elapsed from star formation to the SN Ia events. In this paper, the parameter α is treated as a free parameter that we constrain, while other two parameters are fixed at $\beta = 0$ and $z_{\text{break}} = 1.5$ in our baseline model, in order to reduce the number of free parameters. Although SNe Ia have a time delay from star formation, most DTD models have the peak of the distribution at relatively small t_{Ia} and supernova rate data used in our analysis are at $z \lesssim 1$. Therefore the dependence of our results on β and z_{break} is not large (see §5.2).

4.2. Delay Time Distribution

To test a variety of DTD of SNe Ia, we use the theoretical models constructed by Greggio (2005) for a wide variety of the progenitor models (single or double degenerate, and others). We use four representative models; two of them are based on the single degenerate scenario with two different distributions of the secondary stellar masses adopted in Greggio (2005) or Greggio & Renzini (1983), which are labeled as “SD-G05” and “SD-GR83”, respectively. The other two models are based on the double degenerate scenario with two different treatments of the common envelope phase, which are labeled as “close-DD” and “wide-DD”, respectively.

In addition to these models based on the stellar evolution theory and SN Ia progenitor scenarios, we also test more phenomenological DTD models based on simple functional forms as frequently used in SN rate studies (Madau et al. 1998; Strolger et al. 2004). One is the Gaussian distribution,

$$f_D(t_{\text{Ia}}, \tau_{\text{Ia}}) = \frac{1}{\sqrt{2\pi}(0.2\tau_{\text{Ia}})} \exp \left[-\frac{(t_{\text{Ia}} - \tau_{\text{Ia}})^2}{2(0.2\tau_{\text{Ia}})^2} \right], \quad (4)$$

and the other is an exponential distribution,

$$f_D(t_{\text{Ia}}, \tau_{\text{Ia}}) = \frac{\exp(-t_{\text{Ia}}/\tau_{\text{Ia}})}{\tau_{\text{Ia}}}. \quad (5)$$

All of the above DTD models are shown in Fig. 6.

Recent observations about the dependence of supernova rate on the host galaxy properties (e.g., galaxy type, stellar mass, star formation, radio activity) provide evidences for a significant population of SNe Ia whose rate is directly

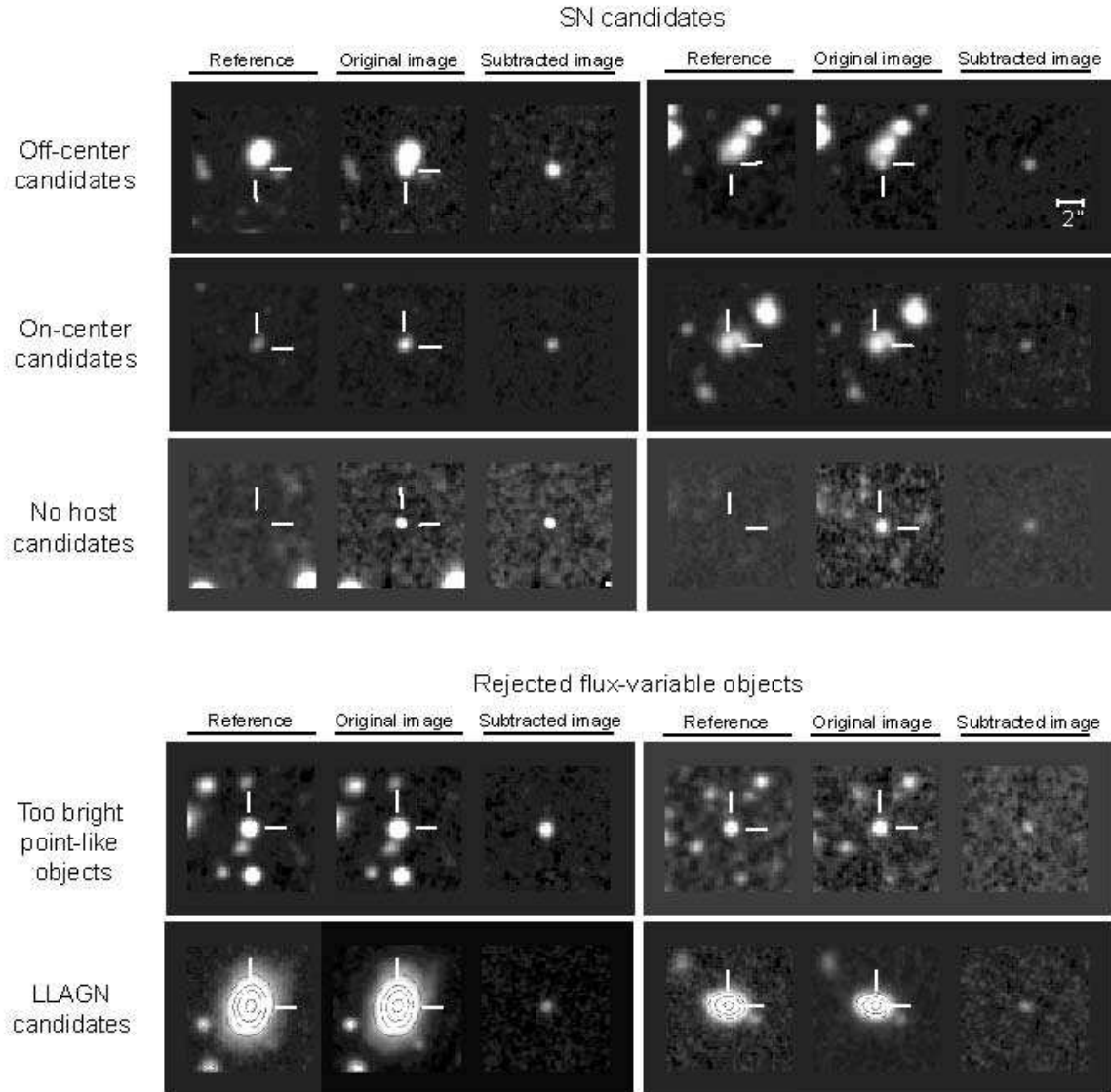


Fig. 4. Images of the supernova candidates as well as rejected objects (see text). In each panel, the left image is the reference (first epoch), the central image is the second epoch image, and the right image is the subtracted image. The positions of variabilities are indicated as the crossing points of two white bars. The scale of this image is shown in the upper right panel.

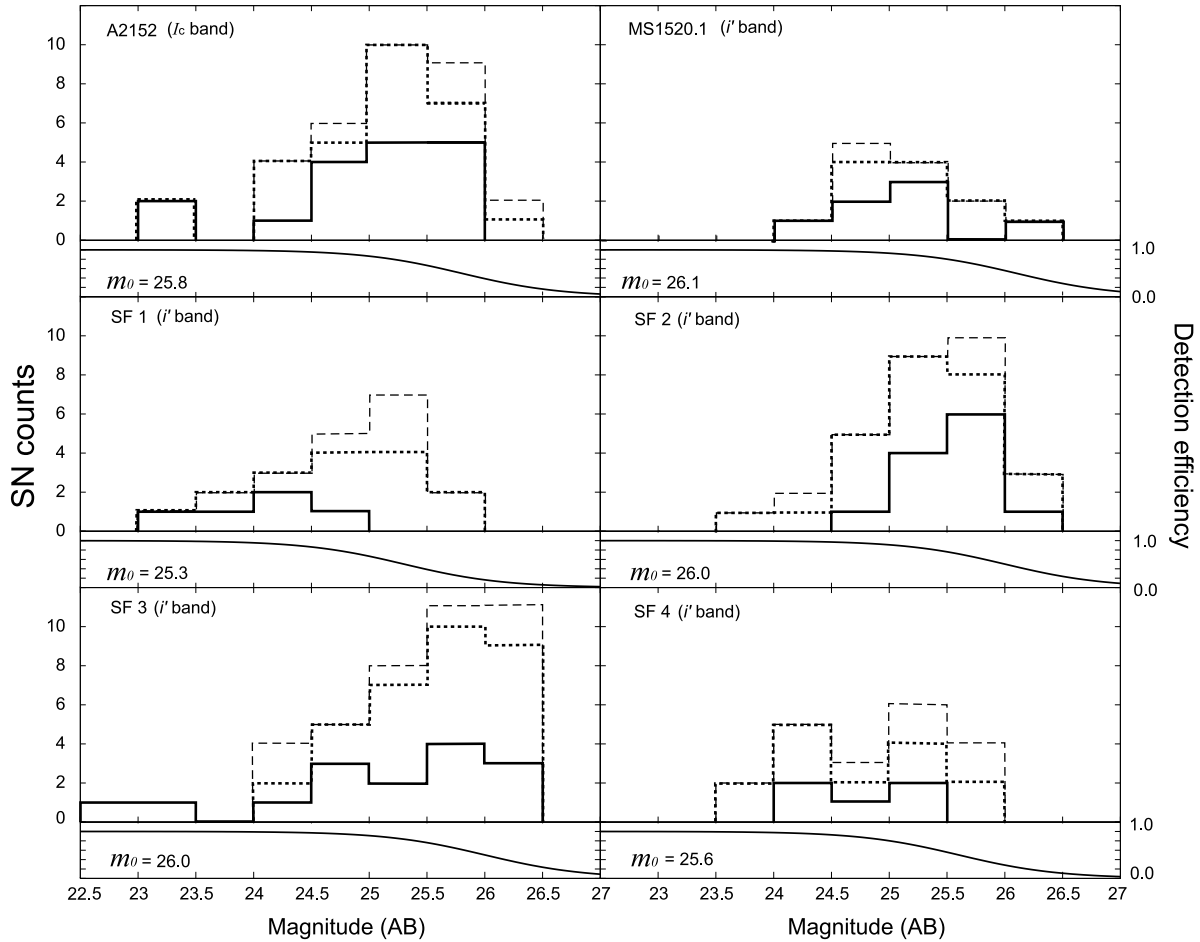


Fig. 5. Variability magnitude (i' or I_c) distributions of the supernova candidates detected in the six different SSS fields. The distributions of the off-center SN sample (solid line), the off-center plus on-center samples (dotted line), and all the samples including the no-host sample are shown. Solid curves in the small bottom panels show the detection efficiency in each field.

proportional to the star formation activity (Dallaporta 1973; Oemler & Tinsley 1979; Della Valle et al. 1994, 2005; Mannucci et al. 2005; Scannapieco & Bildsten 2005; Sullivan et al. 2006; Aubourg et al. 2007). Especially, the correlation with radio galaxies may indicate a bimodal DTD by two distinct populations (Mannucci et al. 2005). To test this possibility, we assume a bimodal delay time distribution which contains the prompt and tardy populations. For the tardy populations we use the DTD models described above, and the combined DTD with the prompt population becomes

$$f_D(t_{\text{Ia}}) = \epsilon_{\text{CSFH}} \delta(t_{\text{Ia}}) + (1 - \epsilon_{\text{CSFH}}) f_{\text{delay}}(t_{\text{Ia}}). \quad (6)$$

Here, the tardy part of $f_{\text{delay}}(t_{\text{Ia}})$ is normalized to the unity when it is integrated over t_{Ia} . We set $\epsilon_{\text{CSFH}} = 0.4$, which has been inferred from observations (e.g., Sullivan et al. 2006). As we will find later, constraints derived by our analysis are mainly for CSFH, and the DTD modeling does not significantly affect our main conclusions. In fact, we find that our conclusions are not significantly changed if $\epsilon_{\text{CSFH}} \lesssim 0.7$, and hence the possible existence of the

prompt population is not important in this work.

4.3. Comparison with the Data

The observed data set with which we compare our theoretical model includes (i) variability magnitudes, redshift, and SN type information of the GOODS supernova survey (Strolger et al. 2004) and a supernova survey in the Subaru Deep Field (SDF-SNS, Poznanski et al. 2007), (ii) variability magnitude distribution of SSS, and (iii) various SN rate density data at $z = 0$ as well as high- z as tabulated in Table 3. The majority of the rate density data are for SNe Ia.

While the shapes of CSFH or DTD have been modeled as above, we treat the overall normalizations of the SN rate density evolution as free parameters, separately for Ia and CC SNe. (See §4.5 for more details of the likelihood method.) Therefore our analysis is free from the uncertainties in converting star formation rate into supernova rate, such as the initial mass function, mass ranges of SN progenitors, or white dwarf explosion efficiency.

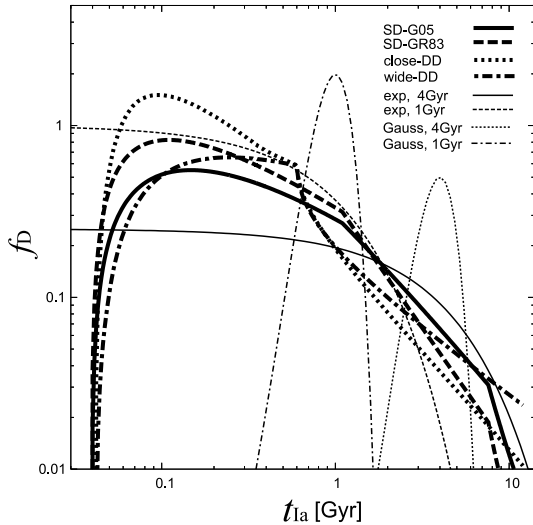


Fig. 6. The delay time distribution function for the type Ia supernova used in this paper. Thick lines show the delay time distribution derived in Greggio (2005), and thin lines show the Gaussian and exponential models.

Table 3. SN rate density data

z	SN rate density [$10^{-4} \text{Mpc}^{-3} \text{yr}^{-1}$]	Reference
Data for SNe Ia		
0.01	$0.28 \pm 0.05^*$	Cappellaro et al. (1999)
0.1	$0.24 \pm 0.12^*$	Madgwick et al. (2003)
0.13	$0.16 \pm 0.07^*$	Blanc et al. (2004)
0.25	0.17 ± 0.17	Barris & Tonry (2006)
0.30	0.34 ± 0.15	Botticella et al. (2007)
0.35	0.53 ± 0.24	Barris & Tonry (2006)
0.45	0.73 ± 0.24	Barris & Tonry (2006)
0.47	0.42 ± 0.06	Neill et al. (2006)
0.5	0.48 ± 0.17	Tonry et al. (2003)
0.55	0.54 ± 0.10	Pain et al. (2002)
0.55	2.04 ± 0.38	Barris & Tonry (2006)
0.65	1.49 ± 0.31	Barris & Tonry (2006)
0.75	1.78 ± 0.34	Barris & Tonry (2006)
Data for CC SNe		
0.01	$0.43 \pm 0.17^*$	Cappellaro et al. (1999)

Note: the rate densities are corrected for the cosmological parameters used in this work.

* The original value has been corrected by using a more recent estimate of the local B-band luminosity density, $\rho = (1.03 + 1.76z) \times 10^8 L_{\odot} \text{Mpc}^{-3}$ (Botticella et al. 2007).

4.4. Dust Extinction

The effect of dust extinction must be taken into account. For comparison with the GOODS, SDF-SNS, and SSS data, we must calculate light curves of various SN types to calculate the expected detection number as a function of variability magnitude. Therefore we first introduce the extinction-corrected light curves of various SN types, and then they are reddened and absorbed by the two parameters of the mean color excess, $E(B-V)_{\text{CC}}$ and $E(B-V)_{\text{Ia}}$ for CC and Ia SNe, respectively. We apply a typical Galactic extinction curve of Cardelli et al. (1989) as the extinction law of both CC SNe and SNe Ia. Some observations indicate that the extinction law of low- z SNe Ia might be different from the Galactic law (Altavilla et al. 2004; Reindl et al. 2005; Wang 2005; Elias-Rosa et al. 2006), but it is still highly uncertain. We confirmed that our results are hardly changed even when the extinction curve of the Small Magellanic Cloud (Gordon et al. 2003) is used. It should be noted that the Calzetti law (Calzetti et al. 2000), which is often used in studies of high- z galaxies, is an empirical law for the effective attenuation (rather than extinction) of flux from a whole galaxy, and is not appropriate for the extinction of flux of a source in a galaxy.

According to the observations of SNe Ia for the cosmological purpose, the degree of reddening for high redshift SNe Ia seems to be similar to those of local SNe Ia (Knop et al. 2003). Thus, we assume $E(B-V)_{\text{Ia}} = 0.05$, which is a typical for local SNe Ia (Altavilla et al. 2004; Reindl et al. 2005), for SNe Ia in all redshifts. This value of $E(B-V)_{\text{Ia}}$ is similar to those used in other SN rate studies. Therefore, we use the reported values of SN Ia rate densities shown in Table 3 in our likelihood analysis. One may expect that the prompt SN Ia population may suffer heavier extinction because generally star forming regions are dusty. However, the inferred time scale of the prompt SN Ia events elapsed from star formation is $\sim 10^8$ yr, which is much larger than the lifetime of massive stars leading to CC SNe.

In contrast, CC SNe could suffer from heavier extinction by dust, and it is also reasonable that the degree of extinction evolves with redshifts reflecting galaxy evolution. We treat $E(B-V)_{\text{CC}}$ as a free parameter for all high- z CC SNe in the analysis of the GOODS, SDF-SNS, and SSS data. On the other hand, we include the local CC SN rate density of Cappellaro et al. (1999) in our likelihood analysis. Comparing the CC SN light curves used in Cappellaro et al. (1999) with those unreddened, the extinction implicitly included in this estimate is $E(B-V) \sim 0.2$. Therefore, if we set $E(B-V)_{\text{CC}} \sim 0.2$, it means that there is no evolution for the mean extinction of CC SNe. Instead, if we get a higher value of $E(B-V)_{\text{CC}}$ by the likelihood analysis, it means that a heavier mean extinction of CC SNe at high redshifts than in the local universe is required. We do not include other CC SN rate density data (e.g., Botticella et al. 2007) than that of Cappellaro et al., because it is difficult to test evolutionary models of $E(B-V)$ by an analysis including various rate density data at different

redshifts that are already corrected for dust extinction with different assumptions.

What we can constrain from the rate density evolution of CC SNe from $z = 0$ to ~ 1 is the combination of α and $E(B - V)_{CC}$. On the other hand, SN Ia rate evolution is affected by α . Therefore, by a combined analysis of CC and Ia SN data, it is expected to be possible to constrain both α and $E(B - V)_{CC}$, if the dependence on DTD is weak. We will show that it is indeed possible.

4.5. The Maximum Likelihood Analysis

Given the theoretical model of SN rate evolution described in the previous section, we can calculate the expected distribution of the variability flux and redshift for each SN type, $d^2N/(dm_{\text{var}}dz)$. This quantity is calculated by the model described in OT05 for a given observation filter, time separation, and detection efficiency of GOODS, SDF-SNS, and SSS data, taking into account a variety of SN light curve templates and colors.

For the GOODS and SDF-SNS, all the information of m_{var} , SN types, and redshift are available. Therefore we use the likelihood function of all the information as:

$$\mathcal{L}_{\text{GOODS/SDF-SNS}} = \sum_j \sum_{i=1}^{N_{\text{obs}}^j} \ln \left[\frac{d^2N_j(m_{\text{var},i}, z_i)}{dm_{\text{var}}dz} \right] - N_{\text{exp}}, \quad (7)$$

where the subscript i is for each supernova, and j denotes the SN types (Ia or CC). The total expectation number N_{exp} is given by

$$N_{\text{exp}} = \sum_j \int dz \int dm_{\text{var}} \frac{d^2N_j(m_{\text{var}}, z)}{dm_{\text{var}}dz}. \quad (8)$$

Note that the likelihood function $\mathcal{L} \equiv \ln L$ is logarithm of the likelihood probability L with an arbitrary additive constant. (See, e.g., Loredo & Lamb 1989 for the derivation of the likelihood function.)

For the SSS data, the type and redshift information is not available, and these are integrated out as:

$$\mathcal{L}_{\text{SSS}} = \sum_{i=1}^{N_{\text{obs}}} \ln \left[\frac{dN_{\text{all}}(m_{\text{var},i})}{dm_{\text{var}}} \right] - N_{\text{exp}}. \quad (9)$$

For SN rate densities in the literature, the likelihood is simply calculated as:

$$\mathcal{L}_{r(z)} = -\frac{1}{2} \sum_i \left[\frac{r_i(z_i) - r_{\text{model}}(z_i)}{\sigma_i} \right]^2, \quad (10)$$

where, r_{model} is SN rate density calculated by our model, and r_i , z_i and σ_i are observed SN rate density, mean redshift, and the statistical errors, respectively, of the i -th data point. These values are summarized in Table 3, after corrected for the cosmological parameters into those used in this paper. As mentioned in §4.4, we use all the rate density data of SNe Ia, but we use only the local rate density of Cappellaro et al. (1999) for CC SNe.

Then, the combined likelihood function for all the data set is given by: $\mathcal{L}_{\text{total}} = \mathcal{L}_{\text{GOODS}} + \mathcal{L}_{\text{SDF-SNS}} + \mathcal{L}_{\text{SSS}} + \mathcal{L}_{r(z)}$. We derive the confidence levels in a standard manner

assuming that $-2\mathcal{L}$ obeys to the χ^2 distribution, and the confidence regions are determined by the contours of $\Delta\chi^2 = \chi^2 - \chi_{\text{min}}^2$ (e.g., Press et al. 1992).

5. Constraints on Parameters

5.1. Constraints on α and $E(B - V)_{CC}$

First we present the confidence regions for α and $E(B - V)_{CC}$, by using the baseline model, i.e., $\beta = 0$, $z_{\text{break}} = 1.5$, and the SD-G05 DTD model (left panel of Fig. 7). In the next subsection we will show that the constraints on these parameters are robust against the other parameters of β , z_{break} , and DTD models within the reasonable ranges. The maximum likelihood is obtained at $[\alpha, E(B - V)_{CC}] = [3.7 \pm 0.5, 0.48 \pm 0.07]$ when we use only the off-center SSS data, while at $[4.2 \pm 0.5, 0.48 \pm 0.07]$ for the case of using both on- and off-center SSS data. The statistical errors of these parameters are calculated by one parameter fitting with the other parameter marginalized. As discussed in §3.5, these two cases should be regarded as the minimum and maximum numbers of on-center supernovae in SSS. However, the difference between these two in this plot is not significant compared with the statistical uncertainties. We will show the results derived from the off-center SSS data as the baseline results in this paper.

Our result indicates $\alpha \sim 4.0$, and also that there is a considerable evolution of mean extinction of CC SNe from $z = 0$ to $z \sim 0.5$ (a typical redshift for CC SNe used in the likelihood analysis). It should be noted that the constraint on α is derived only using supernova data sets, without any information on the other observational estimates of CSFH. Therefore it is interesting to compare our result with CSFH estimates by galaxy surveys. The estimates of α based on UV luminosity density are $\alpha = 1.7 \pm 1.0$ (Wilson et al. 2002) and $\alpha = 2.5 \pm 0.7$ (Schiminovich et al. 2005) without taking into account the evolution of extinction. On the other hand, the estimates based on H α luminosity, which is less sensitive to the dust extinction, are $\alpha \sim 3.5$ (Tresse et al. 2002) and $\alpha = 3.1$ (Doherty et al. 2006). Furthermore, an estimate based on mid-infrared luminosity gives $\alpha = 4.0 \pm 0.2$ (Pérez-González et al. 2005). Therefore, there is a clear trend that the estimate of α becomes smaller for methods that are more seriously affected by dust extinction. (See also Takeuchi et al. 2005.) This trend is nicely consistent with our result; the true SFR evolution to $z \sim 1$ is described by $\alpha \gtrsim 3$, and small α values inferred from UV-based estimates can be accounted for by the increase of mean extinction of star forming regions from $z = 0$ to $z \sim 0.5$.

5.2. Dependence on the Other Parameters

In order to show the robustness of our results against variation of the CSFH model parameters other than α , the constraints derived with different values of z_{peak} and β , as well as the likelihood ratio to the baseline model, are summarized in Table 4. The constraints are almost insensitive to the high- z CSFH index, β , within the reasonable range inferred from galaxy surveys ($\beta \sim -2-0$.) This is because the DTD models based on the stellar evolution

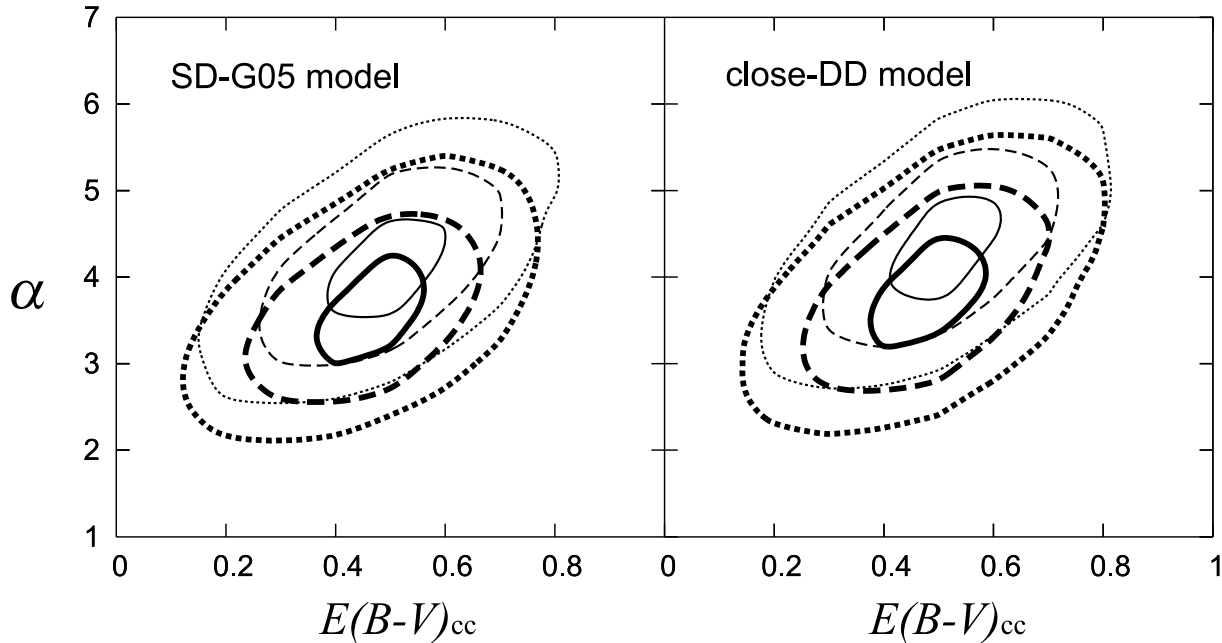


Fig. 7. Confidence regions of the two parameters, α and $E(B-V)_{\text{CC}}$ derived with the SD-G05 (left panel) and close-DD (right panel) models of DTD, respectively. Confidence contours with solid, dotted and dashed curves indicate 68, 95 and 99.7 % (i.e., 1, 2 and 3σ) confidence levels. Thick-lined contours are those derived using only off-center SNe in the SSS sample, while the thin-lined ones are using both on-center and off-center SNe.

Table 4. Constraints on α and $E(B-V)_{\text{CC}}$ and their dependence on z_{peak} and β

	α *	$E(B-V)_{\text{CC}}$ *	Likelihood Ratio †
The baseline CSFH model $[(z_{\text{peak}}, \beta) = (1.5, 0.0)]$			
off-center SSS	$3.7^{+0.5}_{-0.5}$	$0.48^{+0.06}_{-0.07}$	1.0
on & off-center SSS	$4.2^{+0.5}_{-0.5}$	$0.48^{+0.07}_{-0.06}$	1.0
$(z_{\text{peak}}, \beta) = (1.2, 0.0)$			
off-center SSS	$4.0^{+0.4}_{-0.4}$	$0.49^{+0.07}_{-0.07}$	4.1
on & off-center	$4.6^{+0.5}_{-0.5}$	$0.51^{+0.07}_{-0.07}$	5.0
$(z_{\text{peak}}, \beta) = (1.8, 0.0)$			
off-center SSS	$3.5^{+0.4}_{-0.4}$	$0.47^{+0.07}_{-0.07}$	0.5
on & off-center SSS	$3.9^{+0.4}_{-0.4}$	$0.50^{+0.07}_{-0.07}$	0.7
$(z_{\text{peak}}, \beta) = (1.5, -2.0)$			
off-center SSS	$3.7^{+0.4}_{-0.4}$	$0.47^{+0.07}_{-0.07}$	1.2
on & off-center SSS	$4.3^{+0.5}_{-0.5}$	$0.49^{+0.07}_{-0.07}$	1.5

* Errors are statistical 1σ when one of α or $E(B-V)_{\text{CC}}$ is marginalized.

† The ratio of likelihood $L = \exp(\mathcal{L})$ is shown, which is normalized by the value of the baseline CSFH model.

theory have their peak at a relatively short time scale of $\sim 10^8$ yr. The contribution from the prompt SN Ia population makes the effect of changing β even smaller. The constraints do not change significantly within the range of $z_{\text{peak}} \sim 1.2\text{--}1.8$.

To check the dependence on the DTD models, we show the same analysis as above but using the close-DD DTD model in the right panel of Fig. 7. We also show the changes of the constraints when the DTD model is changed from that in the baseline model in Table 5. It can be seen that the derived parameters and the maximum likelihood for various DTD models are very similar, indicating that we can derive a robust constraint on α and $E(B-V)_{\text{CC}}$. Though $\alpha \lesssim 3$ is inferred in the cases of the exponential or Gaussian DTD with a characteristic time scale less than 1 Gyr, such DTDs are rather unlikely, since these cannot explain the fact that SNe Ia occur even in the local elliptical galaxies. On the other hand, we cannot derive any strong constraint on the DTD models, which is consistent with the result of Förster et al. (2006) based on the GOODS data set, while our analysis includes all available data obtained in other SN surveys.

5.3. On the Type Classification Uncertainties

It should be noted that the type determination of the GOODS and SDF-SNS is assumed to be perfectly correct in our analysis. However, SN type determination is not an easy task; in fact, the ‘‘Bronze’’ sample defined in the GOODS (15 out of all 42 SNe) and SNe with intermediate scores of type Ia probability in the SDF-SNS (11 out of all 33 SNe) are thought to be the samples with highly uncertain type classification. To check the uncertainties about this, we analyze the GOODS and SDF-SNS data without using the type information of these SNe. Although the confidence regions are slightly expanded, we obtain almost the same best-fit parameters of α and $E(B-V)_{\text{CC}}$ as those in our baseline analysis. Therefore our results are robust against the type classification in the GOODS and SDF-SNS data set.

5.4. Cosmic SN Rate Density Evolution

Figure 8 shows the best-fit model of the cosmic CC and Ia SN rate density evolution calculated with the SD-G05 model. The best-fit model is in reasonable agreement with the observational data points, but those of the SN Ia rate density at $z \sim 0.6\text{--}0.8$ are significantly higher than the model curve. We investigated various model parameters within our modeling framework, but we cannot reproduce such a high rate density. This indicates that, if the high rate density inferred from the data of Barris and Tonry (2006) and Dahlen et al. (2004) are real, a simple modeling with smooth CSFH and/or DTD models normally applied in the literature are not sufficient. However, other SN Ia rates in the same redshift range [SDF-SNS data and the recent report based on the Supernova Cosmology Project data and the GOODS data (Kuznetsova et al. 2007)] are much lower and consistent with the best-fit model. Strong conclusions cannot be derived for the moment, and more data in this redshift range are highly de-

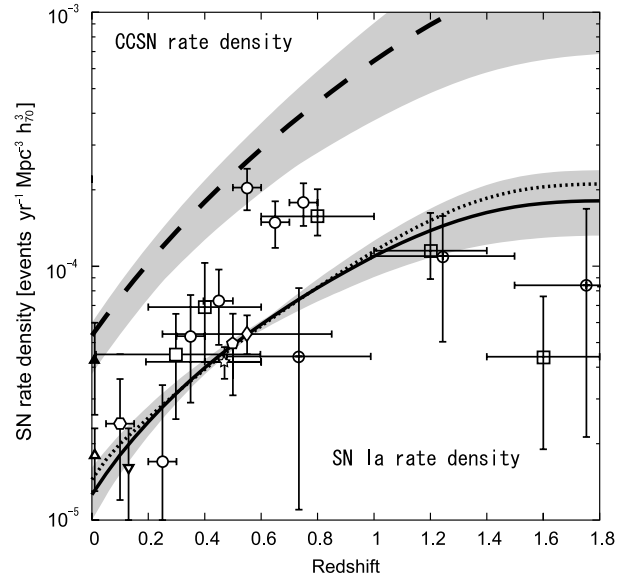


Fig. 8. Time evolution of SN rate density. The solid and dashed lines are our predictions for Ia and CC SNe, calculated from the best-fit parameters in our baseline model. Shaded regions indicate the deviation within the 1σ confidence regions of α and $E(B-V)_{\text{CC}}$ shown in Fig. 7. The dotted line is the same as the solid line, but using the wide-DD DTD model instead of the SD-G05 model. For comparison, data points of SN Ia rate densities used in the likelihood analysis are shown in open symbols: Pain et al. (2002, diamond), Tonry et al. (2003, pentagon), Madgwick et al. (2003, hexagon), Blanc et al. (2004, upside-down triangle), Barris & Tonry (2006, circle), Neill et al. (2006, star), and Botticella et al. (2007, square). The local SN rate densities for Ia and CC SNe (Cappellaro et al. 1999 but corrected as in Botticella et al. 2007) are plotted by open and filled triangles, respectively. We also show Ia rate densities derived from GOODS data in Dahlen et al. (2004, square with cross) and SDF-SNS data in Poznanski (2007, circle with cross), which were not directly used in the likelihood analysis since we used the full redshift and magnitude distributions of these data. High redshift data of CC SN rate density are not plotted since they significantly depend on dust extinction correction.

sirable.

6. Summary and Conclusions

We performed a comprehensive likelihood analysis of almost all available data of the cosmic SN rate density evolution both for CC and type Ia supernovae, to get information on the CSFH and the DTD of SNe Ia. We utilized the variability magnitude and redshift distribution of CC and Ia SNe of the GOODS and SDF-SNS, and other estimates of SN Ia rate density at various redshift in the literature. Furthermore, we added photometrically found supernova candidates in the past imaging data of Subaru/Suprime-Cam (Subaru Supernova Survey, SSS) to increase the statistics. The analysis of the SSS data is newly reported here, including 157 SN candidates down to $i' \sim 26.0$ in the total survey area of 1.4 deg^2 . 61 of the 157 SSS candidates are associated with host galaxies with significant offsets from galaxy centers, and hence they are

Table 5. Constraints on α and $E(B-V)_{\text{CC}}$ and maximum likelihood for different DTD models

	α *	$E(B-V)_{\text{CC}}$ *	Likelihood Ratio †
SD-G05 (the baseline model)			
off-center SSS	$3.7^{+0.5}_{-0.5}$	$0.48^{+0.06}_{-0.07}$	1.0
on & off-center SSS	$4.2^{+0.5}_{-0.5}$	$0.48^{+0.07}_{-0.06}$	1.0
SD-GR83			
off-center SSS	$4.0^{+0.5}_{-0.5}$	$0.50^{+0.06}_{-0.07}$	2.0
on & off-center SSS	$4.6^{+0.4}_{-0.4}$	$0.53^{+0.07}_{-0.08}$	1.6
close-DD			
off-center SSS	$3.8^{+0.4}_{-0.4}$	$0.50^{+0.06}_{-0.07}$	0.7
on & off-center SSS	$4.5^{+0.4}_{-0.4}$	$0.51^{+0.06}_{-0.07}$	0.8
wide-DD			
off-center SSS	$4.2^{+0.5}_{-0.6}$	$0.53^{+0.07}_{-0.07}$	2.0
on & off-center SSS	$4.7^{+0.4}_{-0.4}$	$0.55^{+0.07}_{-0.07}$	2.7
exponential 4 Gyr model			
off-center SSS	$4.3^{+0.5}_{-0.6}$	$0.52^{+0.07}_{-0.07}$	2.7
on & off-center SSS	$4.7^{+0.3}_{-0.3}$	$0.53^{+0.06}_{-0.05}$	5.0
exponential 1 Gyr model			
off-center SSS	$3.1^{+0.4}_{-0.4}$	$0.43^{+0.07}_{-0.07}$	0.7
on & off-center SSS	$3.5^{+0.4}_{-0.5}$	$0.42^{+0.07}_{-0.07}$	1.2
Gaussian 4 Gyr model			
off-center SSS	$4.4^{+0.5}_{-0.6}$	$0.52^{+0.07}_{-0.07}$	0.1
on & off-center SSS	$4.8^{+0.5}_{-0.5}$	$0.56^{+0.06}_{-0.06}$	0.01
Gaussian 1 Gyr model			
off-center SSS	$3.0^{+0.4}_{-0.4}$	$0.42^{+0.07}_{-0.07}$	0.8
on & off-center SSS	$3.2^{+0.4}_{-0.4}$	$0.42^{+0.08}_{-0.07}$	0.5

* Errors are statistical 1σ when one of α or $E(B-V)_{\text{CC}}$ is marginalized.

† The ratio of likelihood $L = \exp(\mathcal{L})$ is shown, which is normalized by the value of the baseline model.

almost certainly supernovae. Though the type and redshift information is not available for SSS, the total SSS SN counts are useful to constrain the poorly known CC SN rate evolution, by a combination with the relatively well determined SN Ia rate evolution.

We have tested a variety of DTD models; some of them are based on the stellar evolution theory, and others are simple analytic functions often used in the literature. It is found that most of DTD models are consistent with the current data set, and hence we cannot set strong constraint on the type Ia SN progenitor.

On the other hand, this rather weak dependence on DTD models is an advantage when one tries to constrain CSFH parameters. It is required that α (the SFR evolution index from $z=0$ to ~ 1) is 3–4, with a considerable evolution of mean extinction of CC SNe, as $E(B-V) \sim 0.2$ at local and $E(B-V) \sim 0.5$ at $z \sim 0.5$. Since we did not utilize any information from CSFH estimates by galaxy surveys, we can compare our result with those by galaxy

surveys. Recent estimates based on UV luminosity are $\alpha \lesssim 2.5$, while those based on $H\alpha$ or mid-infrared luminosity are close to our result, $\alpha \sim 3$ –4. These are nicely consistent with our finding of the significant evolution of extinction for CC SNe, indicating a strong evolution of extinction of star formation activity in the universe even at $z \sim 0$ –0.5.

The consistency between CSFH based on SFR in galaxies and SN rates is not trivial. Most indicators of galactic SFR trace the production of UV or ionizing photons and hence the formation of massive stars, which is the same as CC SNe. However, an evolution of IMF of massive stars could change the ratio of UV photon production to CC SN rate. Our result implies a roughly constant production efficiency of SNe per unit mass of star formation, and this would give some constraint on IMF evolution or metallicity effects. We have also demonstrated that, based on the counts of SN candidates without host galaxies, the contribution to the cosmic star formation activity from faint

galaxies under detection limit or intergalactic star formation should not be significant. This is a clear advantage of CSFH constraint from supernova surveys, which cannot be obtained by CSFH studies based on galactic SFR estimates.

The authors would like to thank L. Greggio for providing the data of delay time distribution and useful discussions. We also appreciate useful comments from A. Gal-Yam, D. Maoz, D. Poznanski, and an anonymous referee. A part of the SSS data was obtained as a part of the Supernova Cosmology Project (SCP), and we also thank the SCP members for useful discussions. This work was supported by the Grant-in-Aid for the 21st Century COE “Center for Diversity and Universality in Physics” from the Ministry of Education, Culture, Sports, Science and Technology (MEXT) of Japan. T.O. has been supported by JSPS Research Fellowships for Young Scientists. T.T., N.Y., and M.D. are supported by the JSPS - USA bilateral programme.

References

- Alard, C., & Lupton, R. H. 1998, *ApJ*, 503, 325
 Alard, C. 2000, *A&AS*, 144, 363
 Altavilla, G., et al. 2004, *MNRAS*, 349, 1344
 Aubourg, E., Tojeiro, R., Jimenez, R., Heavens, A. F., Strauss, M. A., Spergel, D. N. 2007, preprint, (astro-ph/0707.1328)
 Barris, B. J., et al. 2004, *ApJ*, 604, 571
 Barris, B. J., & Tonry L. J. 2006, *ApJ*, 637, 427
 Bartunov, O. S., Makarova, I. N., & Tsvetkov, D. I. 1992, *A&A*, 264, 428
 Bertin, E., & Arnouts, S. 1996, *A&AS*, 117, 393
 Blakeslee, J. P., Lucey, J. R., Barris, B. J., Hudson, M. J., & Tonry, J. L. 2001, *AJ*, 121, 1
 Blanc, G., et al. 2004, *A&A*, 423, 881
 Botticella, M. T., et al. 2007, preprint (astro-ph/0710.3763)
 Calzetti, D., et al. 2000, *ApJ*, 533, 682
 Cappellaro, E., Evans, R., Turatto, M. 1999, *A&A*, 351, 459
 Cappellaro, E., et al. 2005, *A&A*, 430, 83
 Cardelli, J. A., Clayton, G. C., & Mathis, J. S. 1989, *ApJ*, 345, 245
 Dahlen, T., & Fransson, C. 1999, *A&A*, 350, 349
 Dahlen, T., et al. 2004, *ApJ*, 613, 189
 Dallaporta, N. 1973, *A&A*, 29, 393
 Della Valle, M., Rosino, L., Bianchini, A., & Livio, M. 1994, *A&A*, 287, 403
 Della Valle, M., Panagia, N., Padovani, P., Cappellaro, E., Mannucci, F., & Turatto, M. 2005, *ApJ*, 629, 750
 Doherty, M., et al. 2006, *MNRAS*, 370, 331
 Elias-Rosa, N., et al. 2006, *MNRAS*, 369, 1880
 Förster, F., Wolf, C., Podsiadlowski, P., Han, Z. 2006, *MNRAS*, 368, 1893
 Gal-Yam, A., Maoz, D., & Sharon, K. 2002, *MNRAS*, 332, 37
 Gal-Yam, A., & Maoz, D. 2004, *MNRAS*, 347, 942
 Gal-Yam, A., Maoz, D., Guhathakurta, P., & Filippenko, A. V., 2007, preprint (astro-ph/0711.0808)
 Gilliland, R. L., Nugent, P. E., & Phillips, M. M. 1999, *ApJ*, 521, 30
 Gordon, K. D., Clayton, G. C., Misselt, K. A., Landolt, A. U., Wolff, M. J. 2003 *ApJ*, 594, 279
 Greggio, L., & Renzini, A. 1983, *A&A*, 118, 227
 Greggio, L. 2005, *A&A*, 441, 1055
 Hopkins, A. M. 2004, *ApJ*, 615, 209
 Hopkins, A. M., & Beacom, J. F. 2006, *ApJ*, 651, 142
 Howell, D. A., Wang, L., & Wheeler, J. C. 2000, *ApJ*, 530, 166
 Ilbert, O., et al. 2005, *A&A*, 439, 863I
 Knop, R. A., et al. 2003, *ApJ*, 598, 102
 Kuznetsova, N., et al. 2007, preprint (astro-ph/0710.3120)
 Loredo, T. J., & Lamb, D. Q. 1989, *Annals New York Academy of Science*, 571, 601
 Madau, P., Della Valle, M., & Panagia, N. 1998, *MNRAS*, 297, L17
 Madgwick, D. S., Hewett, P. G., Mortlock, D. J., & Wang, L. 2003, *ApJ*, 599, 997
 Mannucci, F., et al. 2005, *A&A*, 433, 807
 Mannucci, F., Maoz, D., Sharon, K., Botticella, M. T., Della Valle, M., Gal-Yam, A., & Panagia, N. 2007, preprint (astro-ph/0710.1094)
 Maoz, D., & Gal-Yam, A. 2004, *MNRAS*, 347, 951
 Morokuma, T., et al. 2007, preprint (astro-ph/0712.3108)
 Miyazaki, S., et al. 2002, *PASJ*, 54, 833
 Neill, J. D., et al. 2006, *A&A*, 132, 1126
 Oda, T., & Totani, T. 2005, *ApJ*, 630, 59 (OT05)
 Oemler, A. Jr., & Tinsley, B. M. 1979, *AJ*, 84, 985
 Pain, R., et al. 2002, *ApJ*, 577, 120
 Pérez-González, P. G., et al. 2005, *ApJ*, 630, 82
 Poznanski, D., et al. 2007, preprint (astro-ph/0707.0393)
 Press, W. H., Teukolsky, S. A., Vetterling, W. T., & Flannery, B. P. 1992, *Numerical Recipes in C* (Cambridge: Cambridge Univ. Press)
 Reindl, B., Tammann, G. A., Sandage, A., & Saha, A. 2005, *ApJ*, 624, 532
 Sharon, K., Gal-Yam, A., Maoz, D., Filippenko, A. V., Guhathakurta, P. 2007, *ApJ*, 660, 1165
 Scannapieco, E., & Bildsten, L. 2005, *ApJ*, 629, 85
 Schiminovich, D., et al. 2005, *ApJ*, 619, L47
 Stocke, J. T., et al. 1991, *ApJS*, 76, 813
 Strigari, L. E., Beacom, J., Walker, T. P., & Zhang, P. 2005, *JCAP*, 04, 017
 Strolger, L., et al. 2004, *ApJ*, 613, 200
 Strolger, L., et al. 2005, *ApJ*, 635, 1370
 Sullivan, M., et al. 2006, *ApJ*, 648, 868
 Takeuchi, T. T., Buat, V., & Butgarella, D. 2005, *A&A*, 440, L17
 Tonry, J. L., et al. 2003, *ApJ*, 594, 1
 Totani, T., & Yoshii, Y., 2000, *ApJ*, 540, 81.
 Totani, T., Sumi, T., Kosugi, G., Yasuda, N., Doi, M., & Oda, T. 2005, *ApJ*, 621, L9
 Tresse, L., Maddox, S. J., Le Fvre, O., & Cuby, J. G. 2002, *MNRAS*, 337, 369
 Wang, L. 2005, *ApJ*, 635, L33
 Wilson, G., Cowie, L. L., Barger, A. J., & Burke, D. J. 2002, *ApJ*, 124, 1258
 Yungelson, L., & Livio, M. 1998, *ApJ*, 497, 168
 Yungelson, L. R., & Livio, M. 2000, *ApJ*, 528, 108